Chapter 5

Palladium-Prussian Blue Nanoparticles; As Homogeneous and Heterogeneous Electrocatalysts

5.1 INTRODUCTION

Prussian blue (PB) and its analogues shows an attractive redox electrochemistry along with possess electrochromic, electrochemically-induced ion exchanging and electroanalytical properties (Róka et al., 2006; Tanaka and Tamamushi, 1995; Tani et al., 1998; Upadhyay and Kolb, 1993). Previous works have highlighted limitations of chemically synthesized PB due to limited processability and nanogeometry available for practical applications (Karyakin and Karyakina, 1999; Karyakin et al., 1995, 1999; Pandey and Pandey, 2012b). For instance, PB-based modified electrodes, for electrocatalytic reduction of H_2O_2, were limited due to the use of electro-synthesized nanomaterials (de Mattos et al., 2000; Karyakin et al., 2004). Therefore, it has been a challenging demand to synthesize PB in generating nanomaterials-based design with a specific application towards H_2O_2 detection. One possible route is the synthesis of nano-sized PB, which is likely to overcome such limitations due to nanostructured material dispersion. Accordingly, an attempt to meet such a requirement has been made that allowed 3-aminopropyltrimethoxysilane (3-APTMS) and cyclohexanone mediated controlled conversion of potassium hexacyanoferrate into Prussian blue nanoparticles (PBN). As synthesized, PBN displayed excellent nanogeometry, polycrystallinity, and processability to use in both homogeneous as well as in heterogeneous systems (Pandey and Pandey, 2013b) with impressive electron transfer rate to the order of 32 s^{-1} as compared to that of many PB systems available in the literature. Appliance of 3-APTMS during the controlled synthesis of polycrystalline PB

and its analogues (Pandey and Pandey, 2013b) may induce auto-hydrolysis, condensation and polycondensation reactions, affecting their bioanalytical applications. An alternative of 3-APTMS is the use of tetrahydrofuran-hydroperoxide (THF-HPO), which acts as a redox agent to synthesize processable PB (Pandey and Pandey, 2014). The resulting PB nanomaterial performed well both as homogeneous and heterogeneous catalysts towards H_2O_2, based on their peroxidase mimetic electrocatalytic activities.

Still, A need of electrocatalyst, comparable to that of natural systems like peroxidases, directed to facilitate nanocomposite formation combining PBN with other metal nanoparticles. As palladium nanoparticles have been considered to be one of the known potent electrocatalysts (Begum et al., 2017) and synthesis of the same has been challenging task. Meanwhile, the organic reducing agent (THF-HPO) enabled the formation of palladium nanoparticles (PdNP) of the desired nanogeometry as a function of 3-APTMS concentrations (Pandey and Pandey, 2014) as reported earlier. Accordingly, this chapter deals with the synthesis of electrocatalyst with peroxidase like activity, illustrating the role of alkoxysilane (3-APTMS) in stabilizing both PBN and PdNP. In this work, we have thus examined the formation of nanocomposites of PBN with PdNP of different nano dimension involving the active participation of THF-HPO that enable homogeneous nanocomposite dispersion with possible synergistic effects of both PBN and PdNP in electroanalytical applications. In addition, such nanodispersion has been manipulated with two different size of palladium nanoparticles ($PdNP_1$ and $PdNP_2$) to yield three different systems: (i) PBN alone, (ii) PB-$PdNP_1$ and (iii) PB-$PdNP_2$. Their peroxidase mimetic activity and glucose detection were firstly investigated by aqueous nano-suspensions. Besides theyapplied for the electrocatalytic sensing of hydrogen peroxide (H_2O_2) in both homogeneousand heterogeneous environment.

5.2 EXPERIMENTAL

5.2.1 Materials

Graphite powder (particle size = 1-2 μm), Nujol oil (density = 0.838 g mL^{-1}), and 3-aminopropyltrimethoxysilane (3-APTMS) were obtained from Sigma-Aldrich Co., India. Potassium ferricyanide, H_2O_2, and tetrahydrofuran (THF) were purchased from Merck, India. THF-HPO was synthesized by autoxidation of tetrahydrofuran (THF). Potassium tetrachloropalladate was purchased from HiMedia, India. All other chemicals used were

of analytical grade. The water used in experiments was double distilled de-ionized water obtained from the Alga water purification system.

5.2.2 Synthesis of PBN and its nanodispersion with PdNP

In a typical procedure, 50 μL aqueous solution of potassium ferricyanide (0.5 M) was mixed with 200 μL of THF-HPO under stirred conditions over a vertex cyclomixer. The mixture immediately turns into a green colour which was left to stand for 12 hours. The colour of the solution turned to light blue, indicating the formation of PBN. As-synthesized PBN was treated with ethyl acetate to eliminate residual organic moiety and collected by centrifugation, followed by washing and drying.

In a typical procedure, PdNP were synthesized by mixing an aqueous solution of K_2PdCl_4 (0.003 M, 50 μL) with 10 μL of two different concentrations of 3-APTMS i.e., 0.5 M and 1.0 M under stirring condition over a cyclo mixer followed by the addition of THF-HPO (15 μl), resulting in the formation of $PdNP_1$ and $PdNP_2$ respectively at the room temperature. The mixture turns into light black colour within <15 min, which subsequently converted into dark black coloured sol named as; $PdNP_1$ and $PdNP_2$ as a function of 0.5 and 1.0 M concentrations of 3-APTMS, respectively. The nanocomposite formation involves the mixing of 100 μl of PBN and 50 μl of $PdNP_1$ or $PdNP_2$ solutions leading to the formation of a homogeneous nanodispersion of PB-$PdNP_1$ and PB-$PdNP_2$ respectively.

The as-synthesized nanocomposite dispersion was used as a homogeneous catalyst or can be adsorbed on graphite powder to fabricate the nanocomposite modified electrodes. Typically, 100 μl of nanocomposite was mixed thoroughly with 250 mg graphite powder and dried at 90°C for overnight in an incubator. The modified carbon paste electrode (CPE) was prepared by using an active paste of graphite with PBN, PB-$PdNP_1$ and PB-$PdNP_2$. The electrode body used for the construction of the graphite paste electrode was obtained from Bioanalytical Systems (West Lafayette, IN; (MF 2010)). Well of the electrode body was filled with an active paste of composition: PBN/PB-$PdNP_1$/PB-$PdNP_2$= 4% (w/w); graphite powder=68% (w/w); Nujol oil =28% (w/w) as shown in Table 5.1. The desired amount of modifier was thoroughly mixed with graphite powder (particle size 12 μm) in a blender followed by addition of Nujol oil. Finally, the paste surface was manually smoothed on a clean butter paper.

5.2.3 Electrochemical Setup

All electrochemical measurements were performed on Electrochemical Workstation Model CHI660B, CH Instruments Inc., TX, USA in an electrochemical cell equipped with a three-electrode configuration having CPE-PBN/CPE-PB-PdNP$_1$/CPE-PB-PdNP$_2$ as working electrode, while platinum and Ag/AgCl as counter and reference electrode respectively in a working volume of 3 ml. The cyclic voltammogram measurements were performed in 0.1 M phosphate buffer at pH-7.0. The amperometric measurement for H_2O_2 electrochemical reduction was executed at 0.0 V vs. Ag/AgCl. Whereas at higher potential (0.6 V vs. Ag/AgCl), the oxidation of H_2O_2 (generated as a function of glucose-oxidase (GOx) catalyzed reaction) was accomplished in 0.1 M phosphate buffer solution (pH-7.0) containing 0.5 M KCl at 25°C. The active electrode surface area were determined by electrochemical measurements as reported earlier (Daubinger et al., 2014; Doña Rodríguez et al., 2000).

5.2.4 Instrumentation and kinetic assay

The absorption spectra of nanoparticles and kinetic measurements were recorded using the Hitachi U-2900 spectrophotometer. Transmission electron microscopy (TEM) was conducted using Hitachi 800 and 8100 electron microscopy (Tokyo, Japan) with an acceleration voltage of 200 kV. The steady-state kinetics associated with the peroxidase mimetic activity was investigated by varying the concentration of H_2O_2 (0-25mM) at a fixed concentration of o-dianisidine (50 μM). The reaction was carried out in 2 ml phos- phate buffer (0.1 M, pH-7.0). The variation in absorbance was monitored in time scan mode at 430 nm (ε= 11.3 mM^{-1} cm^{-1}). The kinetic parameters were calculated by fitting the absorbance data to the Michaelis-Menton equation.

5.2.5 Hydrogen peroxide detection using GOx as homogeneous catalyst

The analysis was performed by using 40 μl of 10 mg mL^{-1} GOx with 200 μL of different concentrations of glucose in 0.1 M phosphate buffer (pH∼7.0) followed by incubation at 35°C for 45 min. After that, 50 μl of o-dianisidine (0.5 mM) was added with 15 μl of PB-PdNP$_2$ and marked up to 2 ml by adding 0.1 M phosphate buffer (pH∼7.0) to the

reaction solution. Later the reaction mixture was incubated at 45°C for 30 min followed by the recording of spectra at the fixed wavelength (430nm).

5.3 RESULT AND DISCUSSION

5.3.1 Investigation of nanoparticles synthesis through UV-Vis spectroscopy

The appliance of common reducing agent (THF-HPO) during PBN and PdNP synthesis directed us to examine the possibility of PB-PdNP formation. Besides, the size of PdNP could be manipulated as a function of 3-APTMS concentration variation. Consequently, two kinds of nanoparticle dispersions (PB-$PdNP_1$ and PB-$PdNP_2$) have been synthesized in view of their possible catalytic activity investigation. It is crucial to validate the formation of PB-PdNP nanocomposite, via retaining the property of PB and Pd both, based on UV-Vis spectroscopy as displayed in Fig. 5.1. Curve (1) shows the absorbance maxima at 680 nm, typical for as-synthesized PBN, and Curve (2) features the characteristics of PdNP (Sheng et al., 2012; Kora et al., 2018). Whereas the Curve (3) represents absorbance as a function of wavelength for PB- PdNP, which reveals the presence of both PdNP and PBN. And the visual photographs (i,ii and iii) shown in the inset of Fig. 5.1 justified the feasibility of stable nanodispersion formation.

5.3.2 TEM analysis

TEM technique characterized the nano-dimension of all synthesized particles. The analysis indicates that the size of palladium particles was influenced by 3-APTMS concentration variation. The different sized nanoparticles; $PdNP_1$ (20 nm, Fig. 5.2A) and $PdNP_2$ (14 nm, Fig. 5.2B) were obtained as a function of 3-APTMS concentrations; 0.5 M and 1M, respectively. Furthermore, particles of PB-$PdNP_1$ (Fig. 5.3(A,B,C)) and PB-$PdNP_2$ (Fig. 5.3(D,E,F)) shows clumped structure with lattice spacing of 0.2 nm and 0.35 nmfor PdNP and PBN (Fig. 5.3 (C,F)) respectively, justifying occurrence of the same. The SAED pattern further revealed face-centered cubic crystal lattice (inset of Fig. 5.3 (A,D)) displaying palladium and PB planes. EDX spectrum and elemental mapping (Fig. 5.4) analysis revealed the presence of Pd, Fe, and Si elements.

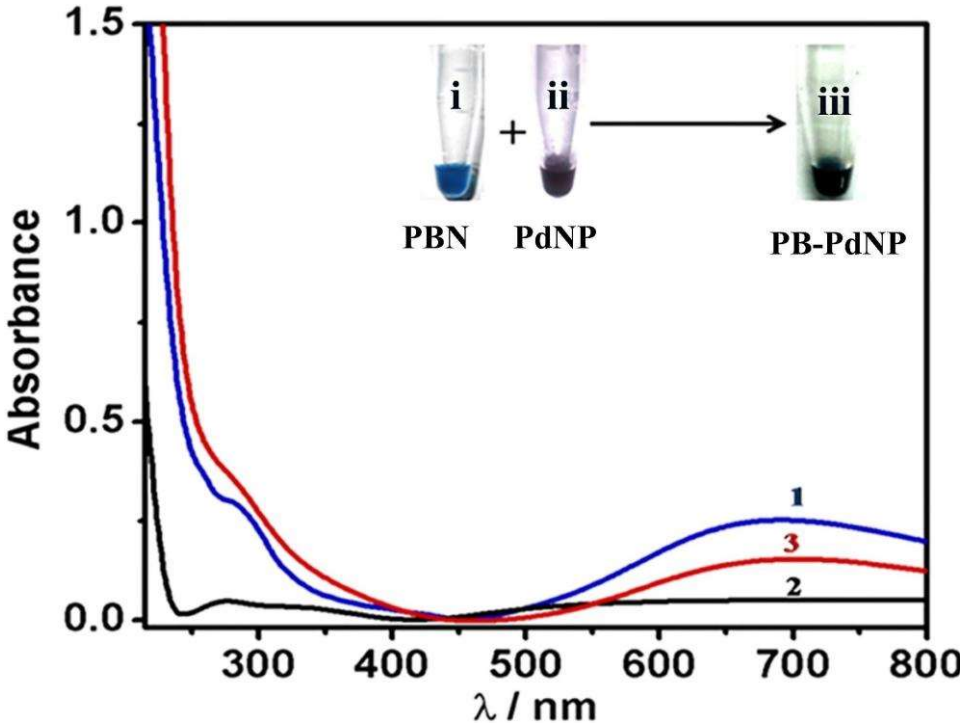

Figure 5.1: Absorption spectra of PBN (1), PdNP (2), and PB-PdNP (3); the visual images (i, ii and iii) of corresponding nanoparticles.

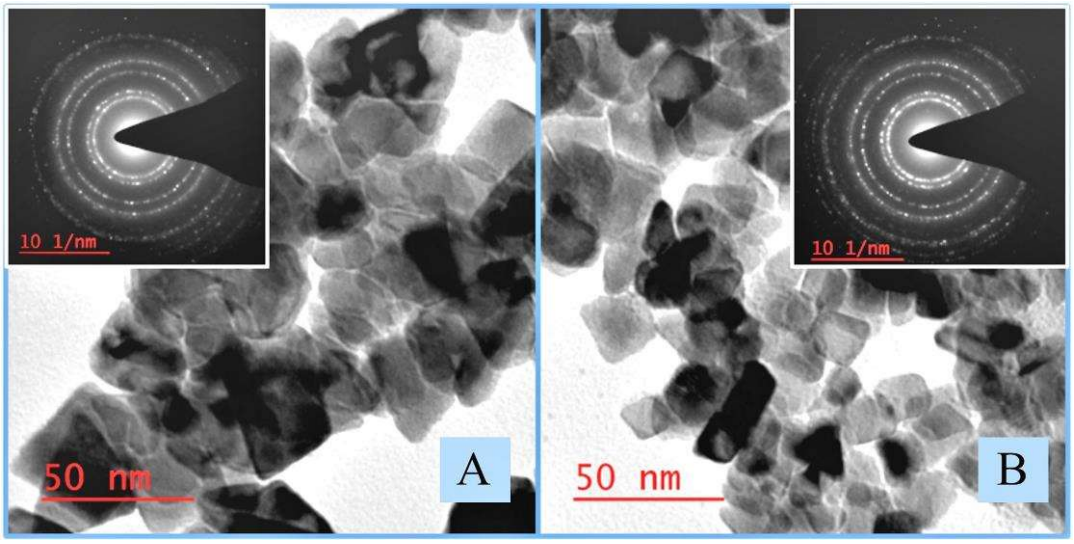

Figure 5.2: TEM and SAED pattern of $PdNP_1$ (A) and $PdNP_2$ (B).

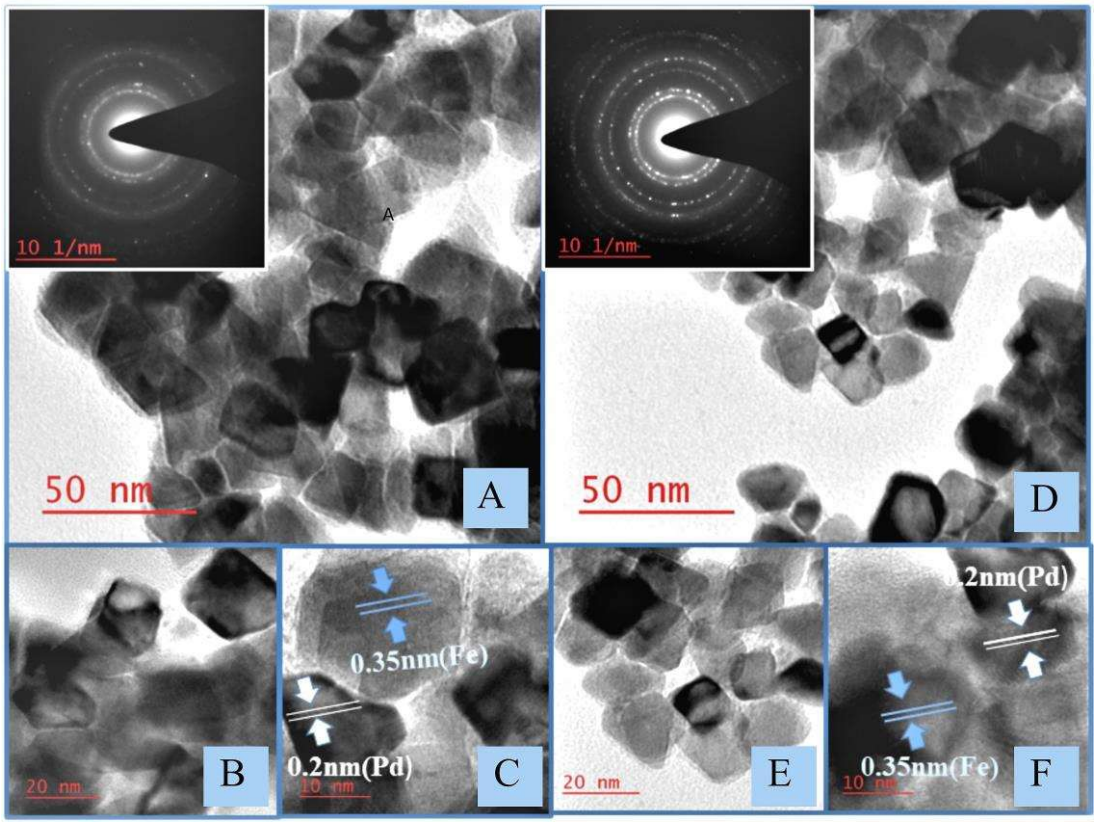

Figure 5.3: TEM images of sequentially synthesized PB-PdNP$_1$ (A,B,C) and PB-PdNP$_2$ (D,E,F) nanoparticles.

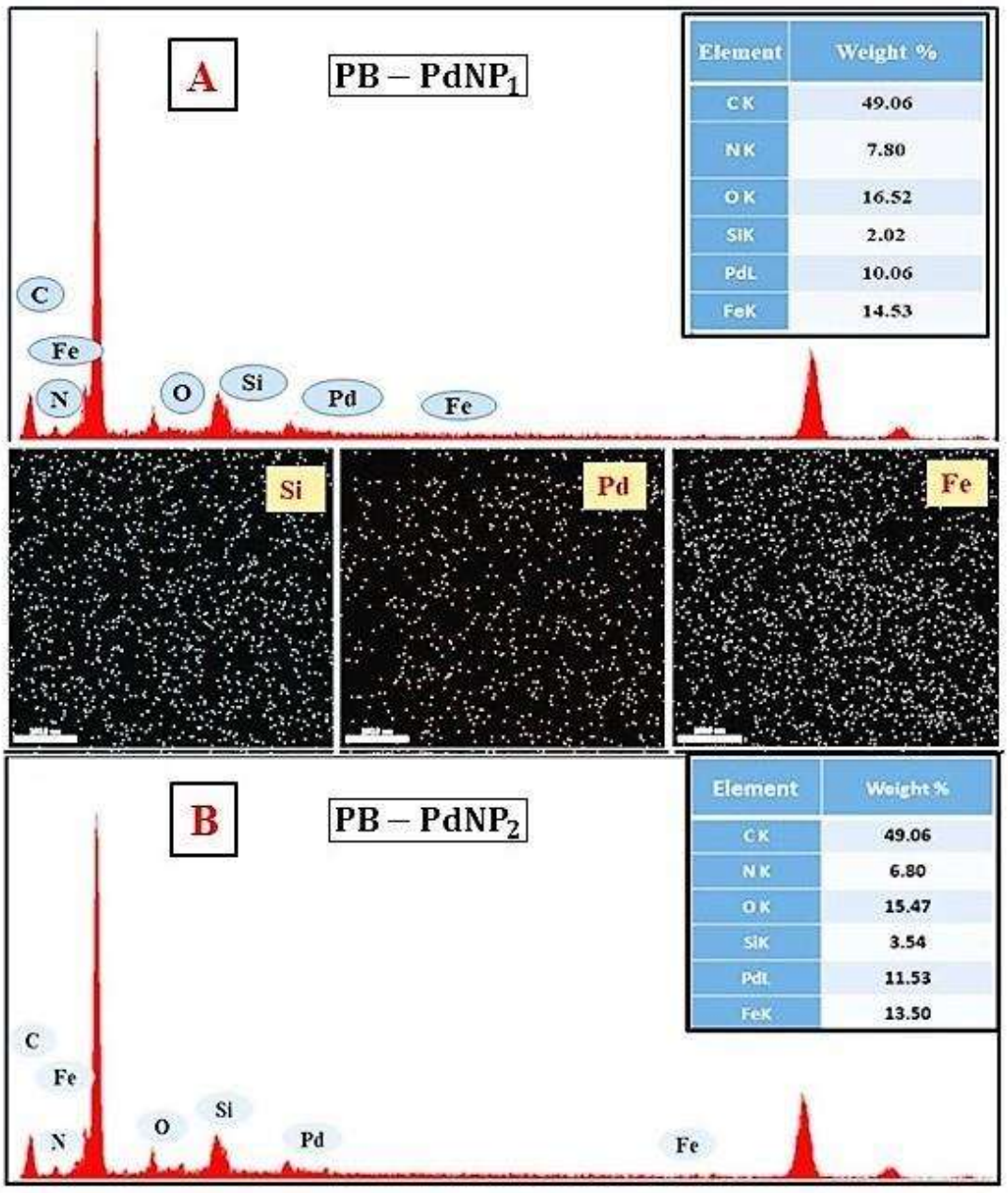

Figure 5.4: Mapping analysis and EDX spectrum of PB-PdNP$_1$ (A), and PB-PdNP$_2$ (B) shows the presence of Fe, Pd and Si elements.

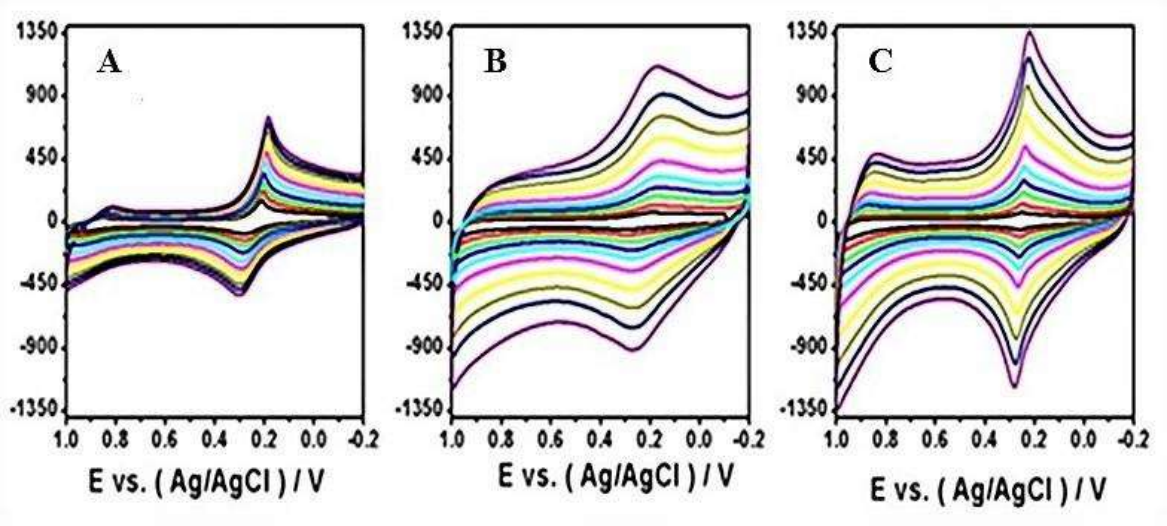

Figure 5.5: Cyclic voltammograms of PBN (A), PB-$PdNP_1$ (B), and PB-$PdNP_2$ (C) at various scan rate of 0.01 to 0.3 Vs^{-1} in 0.1 M KNO_3.

5.3.3 Electrocatalytic behavior of PB-PdNP immobilized on carbon electrode

PB presents a well-defined electrochemical property, having a redox couple at the lower potential of around 0.2 V, corresponds due to the oxidation of Prussian white (PW) and reduction of PB, and the other one at 0.9 V attributed due to the oxidation of PB and reduction of Berlin green (BG) (Karyakin and Karyakina, 1999). THF-HPO mediate structured PB also exhibit similar electrochemical behavior (Pandey and Pandey, 2014) as well as possess an inherent peroxidase mimetic activity (Ricci and Palleschi, 2005). In order to understand the palladium impact over electrocatalytic performance of PBN, modified electrodes have been prepared. Accordingly, three different modified electrodes, i.e., PBN, PB-$PdNP_1$ and PB-$PdNP_2$ have been used to point out the possible influence of palladium nano-dimension over electrocatalytic performance of PBN towards H_2O_2 reduction.

Two reversible redox couples in cyclic voltammograms of the PBN (Fig. 5.5A), PB-$PdNP_1$ (Fig. 5.5B), and PB-$PdNP_2$ (Fig. 5.5C) modified electrodes ware recorded in 0.1 M KNO_3 at the scan rate (0.01 to 0.3 Vs^{-1}) between -0.2 V to 1 V vs. Ag/AgCl. Smaller anodic-to-cathodic peak-to-peak separation, and larger current densities were observed in

PB-$PdNP_1$ and PB-$PdNP_2$ (Fig. 5.5(B,C)) compared to PBN (Fig. 5.5A). It could be explained by facilitating electronic and ionic transport as well as due to enhanced electrode surface area offered by the presence of PdNP. It is vital to resolve the contribution of nanogeometry on the charge transport process. Since $PdNP_2$ is of smaller size compared to that of $PdNP_1$, however the charge transport is found to facilitate at faster rate in PB-$PdNP_1$ as compared to PB-$PdNP_2$ modified electrode. The reason was probably due to the loss of polycrystalline nature at an increased 3-APTMS concentration that possibly retard the dynamics of the charge transport process.

5.3.4 Electrocatalytic reduction of H_2O_2 at modified electrode

Subsequent investigation was attempted in the absence (curve 1) and the presence (curve 2) of 1 mM H_2O_2 to understand the electrocatalytic efficiency of as prepared modified electrodes (PBN, PB-$PdNP_1$ and PB-$PdNP_2$) towards H_2O_2 reduction (Fig. 5.6(A,B,C)). The outcome based on cyclic voltammetry indicates a gradual increase in cathodic current from PB to PB-$PdNP_2$ and justifying the influence of palladium nanoparticle's presence over the nanocomposite. Afterward, an amperometry analysis was performed for H_2O_2 detection (0.01 μM to 5 mM) using PBN, PB-$PdNP_1$ and PB-$PdNP_2$ (Fig. 5.7) modified electrodes, at constant potential (0.0 V vs. Ag/AgCl) in 0.1 M phosphate buffer (pH-7.0). The respective calibration plots (as shown in the inset of Fig. 5.7) indicates the increment in current intensity as a function of H_2O_2 concentration. The sensitivity for H_2O_2 analysis with PBN, PB-$PdNP_1$ and PB-$PdNP_2$ modified electrodes are found to be 109, 222,and 374 $\mu A\ mM^{-1}cm^{-2}$ respectively, confirming better electrocatalytic behavior of PB- $PdNP_2$ as compared to that of PBN and PB-$PdNP_1$. The higher catalytic activity of PB- $PdNP_2$ was attributed to better nanogeometry of $PdNP_2$, demonstrating the formation of a homogenous electrocatalyst retaining the functional activity for practical exploration in both homogenous and heterogeneous phases.

Nevertheless, the palladium's presence significantly enhances the electrocatalytic efficiency of the modified electrodes as recorded from those based on only PB, revealing further the influential role of PdNP during electrocatalysis. Due to the small size of the $PdNP_2$ nanoparticles, there are more sites available for the electrocatalysis, which similarly increase the adsorption of reactants and improve insensitivity. The analytical characteristics previously reported for the catalytic reduction of H_2O_2 using other chem-

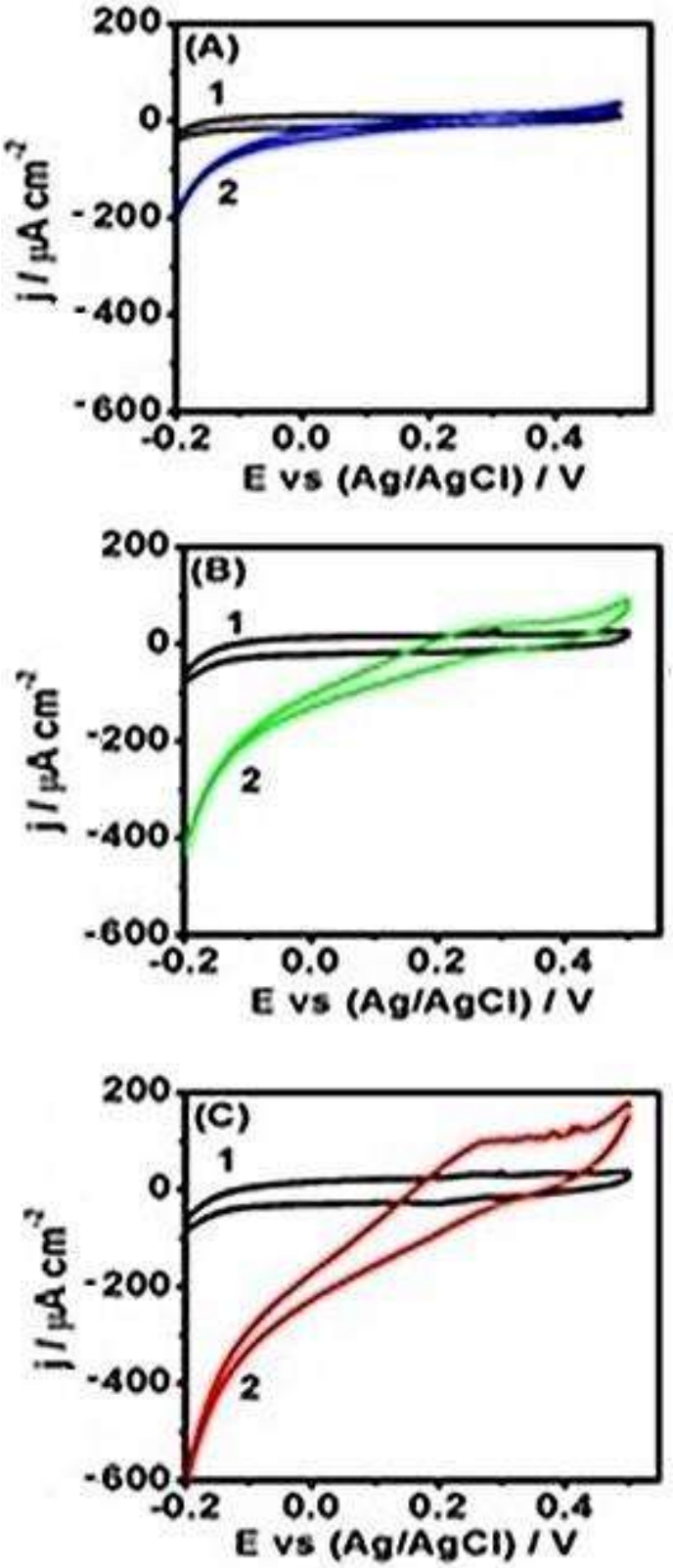

Figure 5.6: Recorded cyclic voltammograms of PBN (A), PB-PdNP$_1$ (B), and PB-PdNP$_2$ (C) modified systems in the absence (1) and presence (2) of 1 mM H_2O_2 in 0.1 M phosphate buffer.

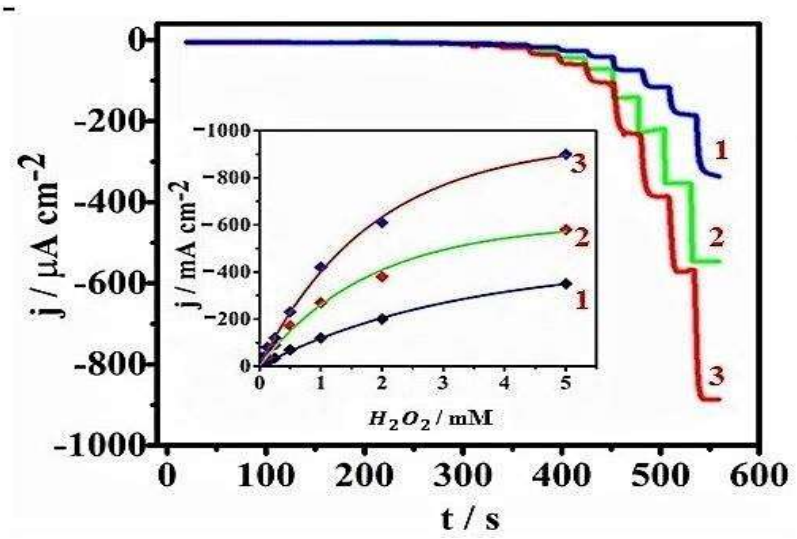

Figure 5.7: Amperometric response of PBN (1), PB-PdNP$_1$ (2), and PB-PdNP$_2$ (3) modified systems, on the addition of varying concentrations of H_2O_2 (0.01 μM to 5 mM) at 0.0 V vs. Ag/AgCl, in 0.1 M phosphate buffer (pH-7.0) containing 0.5 M KCl . Inset shows the corresponding calibration curves for H_2O_2.

---

ically modified electrodes are given in Table 5.1. Comparison of this work with other listed merits, supports the present system and found to be more favorable for H_2O_2 sensing based on the sensitivity measurement under operating potential, and eliminates the possibility of any non-specific electrochemical response.

The peroxidase mimetic catalytic applicability of as-fabricated nanomaterials are examined in a homogeneous medium. Investigation of peroxidase mimetic activity of syn-thesized PB-PdNP$_1$ and PB-PdNP$_2$ was performed using o–dianisidine-H_2O_2 chromogenic reaction. The o–dianisidine substrate turns from transparent to the brown colour in the presence of PB-PdNP composite and H_2O_2, exhibiting an absorbance maxima at 430 nm. Time scan mode is employed to evaluate the kinetics of peroxidase-like activity of the PB-PdNP$_1$ and PB-PdNP$_2$ catalysts (Fig. 5.8(A,B)). The steady-state kinetics were obtained by varying the concentration of H_2O_2 (0.03, 0.08, 0.1, 0.2, 0.4, 0.8, 1.6, 3.2, 6.4, 12.5 and 25 mM) at constant o–dianisidine and catalyst amount. The Michaelis-Menton constant (K_m) of 1.93 mM (Fig. 5.8(A-I)) and 1.71 mM (Fig. 5.8(B-I)) were obtained for PB- PdNP$_1$ and PB-PdNP$_2$ respectively during H_2O_2 detection. This finding indicates that PB-PdNP$_2$ attained more affinity towards substrates as compared to that of PB-PdNP$_1$,

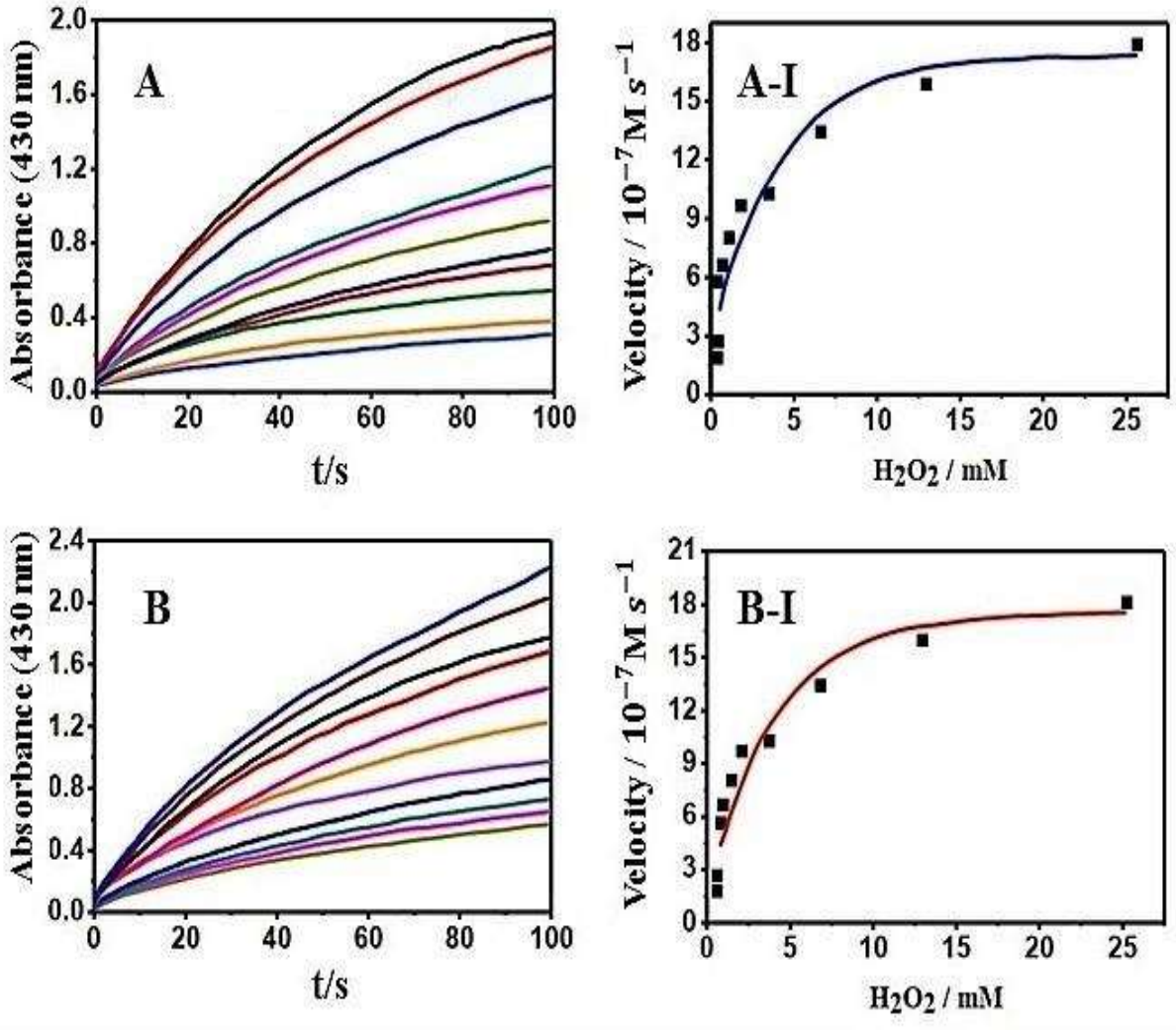

Figure 5.8: Time dependent absorbance variation at 430 nm, depending on H_2O_2 (0.03 to 25 mM) catalytic oxidation by PB-$PdNP_1$ (A), and PB-$PdNP_2$ (B). Kinetic analysis of PB-$PdNP_1$ (A-I), and PB-$PdNP_2$ (B-I) with H_2O_2 as a substrate in phosphate buffer (pH-7.0).

and much higher to PBN (K_m value of 2.98 mM, as reported earlier (Pandey and Pandey, 2014)). Therefore, an increase in the 3-APTMS concentration was observed to enhances

Table 5.1: Comparison of different modified electrodes in the determination of H_2O_2

Substrate	Modifier	Operating Potential/V	Linear Range/μM	Sensitivity $\mu AmM^{-1}cm^{-2}$	Detection limit/ μM	Reference
GCE	PB-Fe_2O_3	-0.15	20-300	7.27[a]	11	(Dutta et al., 2012)
CPE	FMCA-sol-gel-HRP	-0.10	Nr	30	Nr	(Pandey et al., 2003a)
ITO	$[PAH/PB@Au]_n$	-0.10	0.1-100	Nr	Nr	(Qiu et al., 2007)
GCE	PB/POPD	-0.05	0.1-120	2800	0.05	(Ping et al., 2011)
GCE	PBN/Nafion	-0.05	10-6000	138.6	1	(Haghighi et al., 2010)
GCE	CR-GO	-0.20	2.1-140	Nr	0.05	(Zhou et al., 2009)
Pt	SAPB	-0.05	1-400	625	Nr	(Liu et al., 2009)
CPE	Sol-gel-ferrocene/HRP/sol-gel	0	3-57	67[a]	0.6	(Chut et al., 1997)
GCE	SM-Au/PB	0	1-4.5	512	1	Lu et al., 2018
GCE	PB/FG	0.10	1-6	350	1.04	Huang et al., 2019
GCE	PB/NPG	0	1-1.7	708	0.22	Huang et al., 2019
GCE	Ni-Fe-PBA HNCs	0.20	100-20000	36.13	0.29	Niu et al., 2019
Pt	PB-GNPs/BG/GC	0	8100-143000	740	3.2	Keihan et al., 2020
CPE	PBN	0	0.5-1000	108.8	0.2	This work
CPE	$PB-PdNP_1$	0	0.2-1000	221.6	0.1	This work
CPE	$PB-PdNP_2$	0	0.1-1000	374.1	0.1	This work

[a] $\mu A\ mM^{-1}$; Nr= not reported; GCE = glassy carbon electrode; CPE = carbon paste electrode; PAH = poly(allylamine hydrochloride) AuNP = gold nanoparticles; CR-GO = chemically reduced graphene oxide; ITO = indium tin oxide; PBN = Prussian blue nanoparticles;

the material's catalytic activity as the function of particles size. The result also shows that the material is promising for peroxidase replacement. The Michaelis constant (K_m) and the maximal reaction velocity (V_{max}), listed in Table 5.2, justifying the advantage of the present nanomaterial over the previous findings.

5.3.5 Glucose detection using GOx in homogeneous system

glucose sensing was performed through spectroscopic method utilizing o-dianisidine as a chromogenic substrate, analogous to the earlier reported process (Washko and Rice, 1961). The H_2O_2, generated as a function of GOx catalyzed oxidation of glucose, underwent catalytic oxidation in the presence of PB-$PdNP_2$ and produced a coloured oxidized product of o-dianisidine to measure the concentration of glucose. A typical glucose concentration-response curve (Fig. 5.9A) and their corresponding calibration plot (Fig. 5.9(A-I)) have been obtained. The linear range and lowest detection limit (LOD) for glucose were found to be 0.81-12.5 mM and 0.41 mM, respectively.

5.3.6 Glucose sensing based on GOx and PB-$PdNP_2$ modified electrode

The as-prepared PBN and PB-$PdNP_2$ nanocomposites have been examined for electro-catalytic probing of GOx catalyzed reaction. The enzyme electrode was fabricated by incorporating PB-$PdNP_2$ on graphite powder along with GOx. The display voltammograms of PBN (Fig. 5.10A) and PB-$PdNP_2$ (Fig. 5.10B) modified electrode was recorded in the absence and presence of 200 mM glucose. Surprisingly, the modified electrodes responded differently once the addition of glucose has been introduced (Fig. 5.10). An increase in anodic current, near to 2^{nd} redox couple, was observed after the glucose addi- tion in PBN and PB-$PdNP_2$ modified electrodes system. In addition, a five-fold increase in anodic current is recorded, on the addition of similar glucose concentrations, at the sur-face of PB- $PdNP_2$-GOx modified electrode compared to that recorded for only PBN-GOx

Table 5.2: Comparison of the calculated kinetic parameters for PB-PdNP with earlier reported materials.

System	K_m/mM	V_{max} / M s-1	Reference
Fe_3O_4 nanoparticle	154	$9.78x10^{-8}$	(Gao et al., 2007)
PB/-Fe_3O_4	323.6	$1.17x\ 10^{-6}$	(Zhang et al., 2010b)
FeHCF	9.038	$8.40x10^{-7}$	(Pandey and Pandey, 2013b)
Mn-FeHCF	5.64	$8.69x10^{-7}$	(Pandey and Pandey, 2013b)
PB-Ferritin	11.984	$7.20x10^{-7}$	(Zhang et al., 2013)
HRP	3.7	$8.71x\ 10^{-8}$	(Gao et al., 2007)
BiW_9Cu_3	0.29	$0.69x10^{-6}$	(Chai et al., 2015)
Carbon Nanomaterial	0.01	$10.31x10^{-6}$	(Zeng et al., 2017)
Au@HMPB	88.72	$0.25x10^{-6}$	(Zhou et al., 2019)
PB-$PdNP_1$	1.93	$17.36x10^{-7}$	(This work)
PB-$PdNP_2$	1.71	$19.14x10^{-7}$	(This work)

modified electrode. As glucose implies H_2O_2 formation during GOx mediated oxidation of itself at the surface of PBN and PB- $PdNP_2$ modified electrode. The in-situ generated H_2O_2 could undergo in both; the direct and catalytic oxidation at the surface of these electrodes as justified from the results (shown in Fig. 5.10(A,B)).

An increase in anodic current, between 0.5 to 1.0 V vs. Ag/AgCl, after the addition of glucose supports the occurrence of both direct and catalytic oxidations of H_2O_2. In order to have more insight into the mechanistic approach, amperometric glucose biosensing (Fig. 5.10(C, D)) was conducted at the surface of these enzyme-modified electrodes at +0.6 V potential vs. Ag/AgCl, where only electrocatalytic oxidation of H_2O_2 is possible. The other reported PB system could able to catalyze H_2O_2 oxidation athigher potential i.e.> 0.9 V vs. Ag/AgCl with reasonable low sensitivity (Karyakin, 2001;Karyakin et al., 1995).

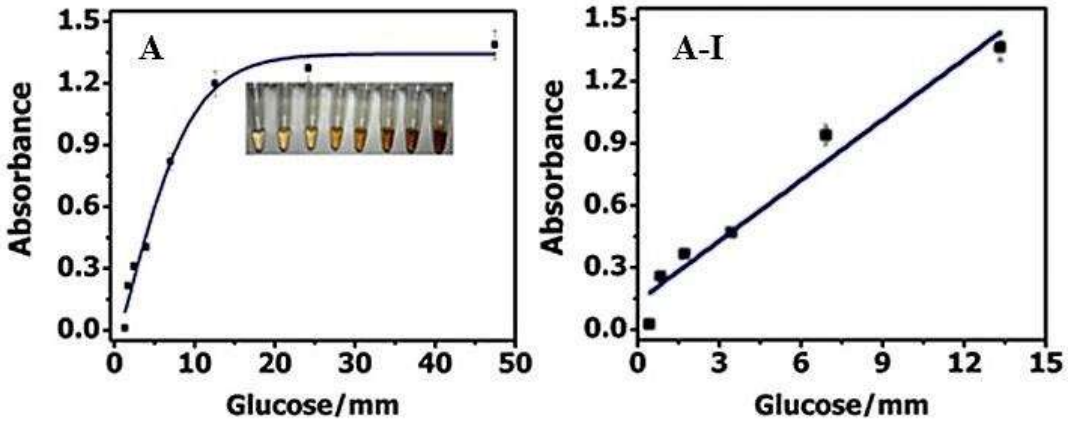

Figure 5.9: Concentration-response curve for glucose detection using GOx enzyme and o-dianisidine in the presence of PB-PdNP$_2$ (A). The linear calibration curve of glucose (A-I).

The amperometric response recorded at + 0.6 V vs. Ag/AgCl indicates better sensitivity of PB-PdNP$_2$ modified electrode as compared to PBN modifiedenzyme electrode and thus concluding the better electrocatalytic characteristics of these nanocomposite modified electrodes. The present configuration of the enzyme electrode offers promising approach as compare to other enzyme electrodes based on H_2O_2 detection.

5.3.7 Stability and reproducibility of modified electrodes

The storage stability of the present systems was studied over four months while keeping the electrodes in phosphate buffer (0.1 M, pH-7.0) at room temperature. After storing for such a long time, decreases of 5-8% were observed in amperometric response of the electrodes. Cyclic voltammetry was also performed to examine the operational stability of the PB-PdNP electrodes. In this case, peak currents and peak potentials remained almost unchanged. However, a decrease in signal was observed after the repetitive 50 cycles at the scan rate of 20 mV s^{-1} towards similar electrode material.

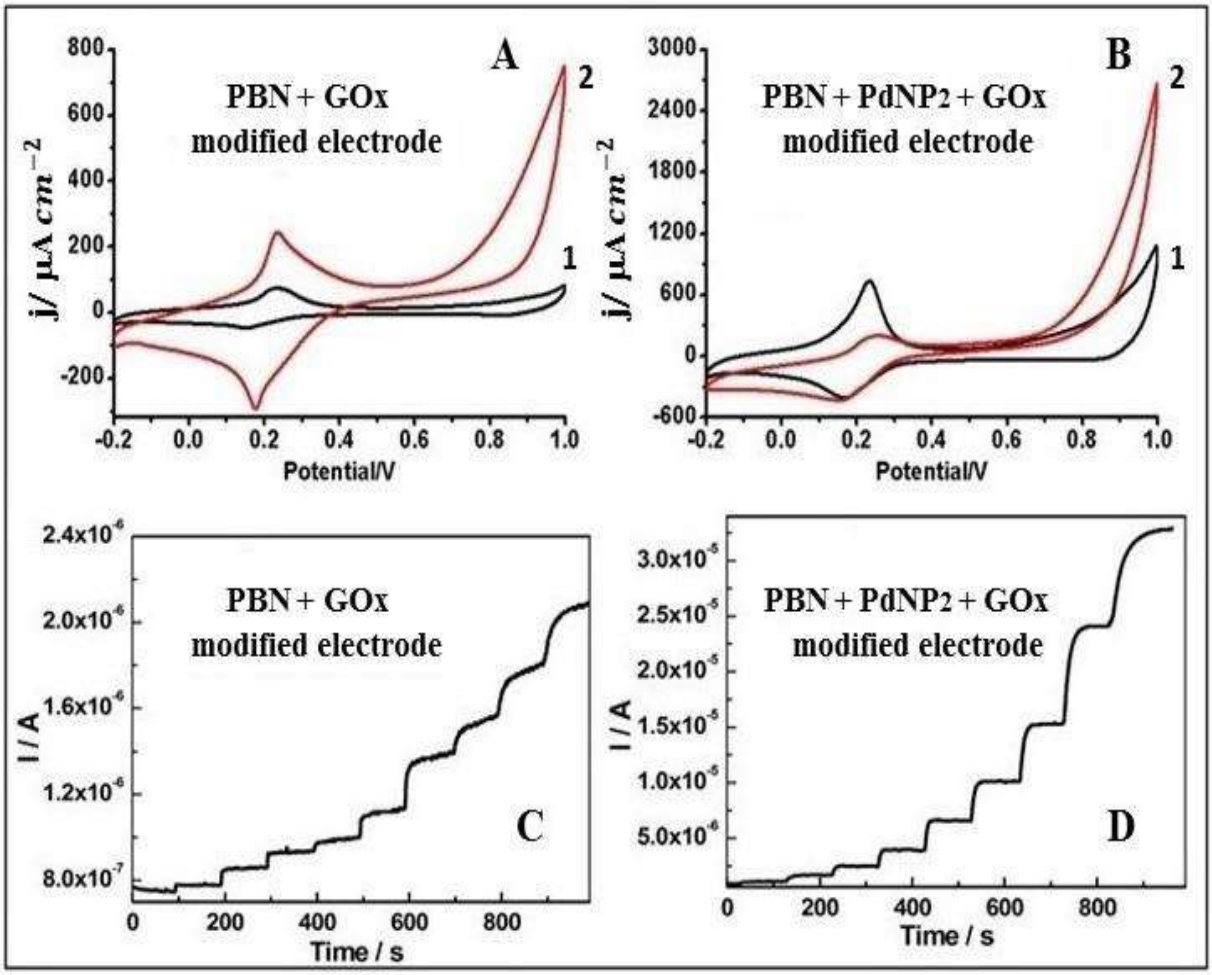

Figure 5.10: Cyclic voltammetry of PBN-GOx (A) and PB-PdNP$_2$-GOx modified enzyme electrode (B) in absence (1) and the presence (2) of 200 mM glucose in 0.1 M phosphate buffer (pH 7.0) at the scan rate of 10 mV/s. Amperometric responses recorded upon addition of increasing concentrations of glucose for PBN (C) and PB-PdNP$_2$ (D) modified enzyme electrodes at constant potential of +0.6 V vs. Ag/AgCl in 0.1 M phosphate buffer (pH 7.0).

The relative standard deviation (RSD) of 3.7 % was recorded during the successive (20) current response measurements of 1 mM H_2O_2 at 0.0 V vs. Ag/AgCl. All these data indicate an excellent stability and reproducibility of PB-PdNP$_2$ systems when applied to the H_2O_2 electrochemical sensing.

5.4 CONCLUSION

In summary, we investigated the possibility of mixing PBN and PdNP of variable nano-geometry to allow the formation of nanodispersion, which displayed the catalytic activity as a function of palladium in both homogeneous and heterogeneous phases. The role of palladium of variable size has also been examined during the electrocatalytic sensing of H_2O_2. The results demonstrate that the presence of Pd in the PB-PdNP nanodis- persion significantly enhances the nanomaterial's electrochemical properties with further improvement in electrocatalysis as a function of nanogeometry of palladium while keeping the similar PBN inherent property in both cases.